Application of the Blister Test to the Study of Polymer–Polymer Adhesion

Y. Z. CHU and C. J. DURNING*

Department of Chemical Engineering and Applied Chemistry, Columbia University, New York, New York 10027

SYNOPSIS

This article demonstrates the use of the blister test for measuring the fracture energy, G_a, of the interface between two incompatible polymers. We describe an apparatus in which a fluid was injected at constant rate at the interface between a solid, glassy polymer, and a thin rubbery overcoating to create a "blister." The fluid pressure and blister geometry were measured as functions of time. An energy balance analysis reveals three independent methods for the calculation of G_a from the data. The method was applied to the system of polyisoprene/poly(methylmethacrylate). We used a sequential debonding procedure to obtain reproducible data following the theoretical predictions. The self-consistency of the data suggested that the adhesion energy could be calculated reliably from the pressure alone, without using the blister geometry.

INTRODUCTION

The adhesion of polymers to a variety of substrates is of great technological importance. Many polymer systems, such as polymer blends, composites, and laminates, include polymer/polymer or polymer/substrate interfaces, whose integrity determines their commercial viability. In order to understand and improve such systems, one needs accurate methodologies for characterizing the mechanical strength of the interface. In this work, we describe a method for polymer/polymer interfaces where one component is glassy and the other is rubbery.

A number of techniques have been developed to quantify the adhesive strength between polymeric films and rigid substrates. For a deformable adhering layer, peel tests are the most common. However, peel tests have many drawbacks, which have been discussed at length in the literature.[1] The main limitation is that the majority of mechanical energy supplied in peeling is dissipated or stored in deforming the test specimen; relatively little energy actually contributes to the fracture process. Consequently, the material property of fundamental importance, namely the fracture energy G_a, is difficult to extract from peel test data.

An alternative method, discussed by Gent and Lewandowski,[2] is the blister test. The test specimen consists of a perforated substrate with a thin flexible overcoating. A fluid is injected at the interface through the perforation, thereby causing a progressive debonding of the overlayer. Gent and Lewandowski[2] have discussed how the adhesion energy can be calculated from the geometry of the blister and the fluid pressure. The blister test offers several advantages over peel tests: (1) there is no direct mechanical contact via fixtures or clamps to effect debonding, (2) the small detachment angle and relatively low debonding rates minimize the dissipative effects in the overlayer (see below), (3) the fracture surface is axisymmetric, which minimizes the effect of sample nonuniformity, and (4) the applied forces are uniform and symmetric without requiring tedious alignment. Adhesion measurements by the blister test were first done in 1961.[3] Recently, the test has been reanalyzed and applied to rigid substrates covered by adhesive tapes[2,4] and thin polymer films, such as polystyrene[5] and polyimides.[6] Unfortunately, the blister test has not been widely used, despite its many favorable features. Because of this, there remains considerable room for improvement of the test, both in the theoretical analysis and the experimental protocol.

* To whom correspondence should be addressed.

Journal of Applied Polymer Science, Vol. 45, 1151–1164 (1992)
 CCC 0021-8995/92/071151-14$04.00

This article describes an application of the blister test to a polymer–polymer system. An important issue addressed is how to perform the experiment so as to minimize the effects of mechanical dissipation during the experiment. Peel tests clearly reveal that the apparent fracture energy for polymer junctions depends strongly upon the peel rate. For example, Gent et al.[7,8] observed for the peel tests on rubber/substrate systems, such as polybutadiene/glass, that the apparent fracture energy for adhesive failure increases by as much as an order of magnitude for a tenfold increase in peel rate. This can be explained by a detailed analysis of the peel force vs. peel rate relation,[8,9] based on energy considerations. The energy expended in peeling is the sum of the reversible work, needed to separate the interface, and a rate-dependent, dissipative part, which typically dominates the peeling energy. This dissipative part includes the rate of work expended to cause flow and/or plastic deformation of the overlayer and substrate, and the energy used to effect pullout or scission of chains at the crack tip. The rate of these processes increases with the crack tip velocity, that is, with the peel rate. Consequently, more energy is dissipated at larger peel rates, leading to an apparent fracture energy increasing with peel rate. During a blister test, the instantaneous debonding rate controls the intensity of dissipative processes. For a test carried out at a constant fluid injection rate, the debonding rate changes, being initially quite large and becoming smaller as the blister grows. One reason for this is geometric: the radial growth rate of a blister, whose volume increases at a constant rate, decreases continuously as the blister grows. (This point is clear if one considers eq. (A–12) in the Appendix, which gives the time dependence of the blister radius a in a constant rate of inflation experiment. From this equation, one finds $da/dt = \text{const}/a^2$ for the instantaneous debonding rate, which indicates that the initial debonding rate da/dt can be large when the blister is small. On the other hand, as the debonding process proceeds, a^2 increases rapidly, thus causing a rapid decrease in da/dt). Another factor leading to large initial debonding rates is that a relatively high initial "critical" pressure is often encountered, that is, the pressure at which the debond first initiates is often much larger than subsequent pressures. This causes "ballistic" debonding initially, where inertia dominates. Thus, one typically finds large initial crack tip velocities in the blister test and one therefore expects large dissipative contributions to work done in the initial portion of the blister test. Indeed, blister tests often yield larger apparent fracture energies from data taken earlier in an experiment.[2] One suggestion for avoiding this is to use the initial critical pressure to characterize the adhesion energy.[5,6,10] The main difficulty inherent in this approach is that it is not clear that this pressure, which characterizes the interface strength in the vicinity of the substrate perforation, is representative of that for the undisturbed interface.

In what follows, we describe a measurement procedure that circumvents the problems associated with large initial rates and critical pressures. With this procedure, the blister test data follow the predictions of a quasi-steady linear–elastic analysis, which completely ignores dissipative effects, indicating that the dissipative effects that are present do not have a dramatic effect on the experimental characteristics. Furthermore, the blister test data are found to be reproducible and self-consistent. The self-consistency indicates that adhesion energies can be calculated reliably from pressure data alone.

EXPERIMENTAL

Sample Preparation

Solid plates of poly(methylmethacrylate) (PMMA) (CYRO Industries, MW $\approx$ 100,000) with dimensions $75 \times 75 \times 5$ mm^3 were used as substrates. Each plate was drilled with a central hole about 5 mm in diameter. The hole was filled with heavy silicon vacuum grease. Then, a cis-polyisoprene (NR) (Scientific Polymer Products, Inc., MW $\approx$ 800,000) hexane solution was spun on the base to create a continuous overlayer with a clean, sharp interface. In order to make the overcoating relatively thick, the NR solution was recast again with a casting knife. Samples were dried slowly at first in a small, covered container to prevent bubble and rough surface formation. This was followed by drying at room temperature in air. The final overcoating of NR had a thickness of about 0.2 mm. Lastly, an elastic tape (Rubbermaid Inc.) about 0.05 mm thick was adhered to the top of the overcoating to provide mechanical reinforcement.

Measurement of Young's Modulus of the Overlayer

The Young's modulus of the overlayers was measured using an Instron Table Model Tester at a strain rate of 0.06 mm/sec, corresponding to the approximate rate of extension of the overlayers in the blister experiments described later. The aver-

age value of the Young's modulus is 1.02 ± 0.08 $\times 10^7$ N/m^2.

Apparatus

Figure 1 shows an overall schematic diagram of the apparatus: A syringe pump (A) (Harvard Apparatus, Inc., model 44) compresses a fluid and pumps it at constant rate into the sample holder (B). The sample holder includes a pressure transducer (C) (OMEGA, model 302) in contact with the fluid. The pressure transducer's output is conveyed to a digital indicator (D), and to an IBM PC–AT computer (E), equipped with data acquisition hardware and software. The sample is viewed with a video camera (F). The tapes can be analyzed for the blister geometry in an image analysis system (G), equipped with JAVA (Jandel Video Analysis Software, Jandel Scientific) software.

Figure 2 shows a schematic of the sample holder (B). The stainless steel holder includes a central hole of about 3 mm in diameter, which conveys the fluid to the hole in the sample base (Fig. 3). A small O-ring (8 mm diameter) seals the working fluid. A second, larger O-ring (38 mm diameter) seals a vacuum port machined into the holder between the O-rings. With the vacuum port connected to a lab source, the sample is securely held in place while the fluid under pressure is pumped through the central hole to debond the overlayer. In all the tests reported, distilled water is the working fluid.

Procedure

First, in order to remove air in the system, fluid is pumped into the holder until the space within the central O-ring and between the two O-ring becomes filled and begins to overflow. The sample is then carefully pressed onto the two O-rings. With the fluid still pumping, the valve connected to the vacuum source is gradually opened. The vacuum clears the fluid between the two O-rings and firmly secures the sample on the holder with no air trapped in the central channel.

In every test, two constant flow rates are applied in sequence by the pump. First, a very small rate, 0.05 mL/min, is used. The NR film inflates to form a small blister with increasing pressure and height, but without debonding. After reaching the initial critical pressure, debonding starts at a relatively high rate and the pressure decreases rapidly as the blister grows. As mentioned in the introduction, the initial rapid debonding is caused by two effects: geometric and ballistic. When the blister has become sufficiently large and the pressure drops to a sufficiently low value, the debonding process is repeated. The flow rate is changed to a larger value, 0.5 mL/min. The pressure increases again to another critical pressure and then falls more gradually than in the first debonding. The radius of this larger blister grows relatively slowly with the pressure gradually decreasing. During each test, the pressure is recorded as a function of time. Also, the geometry of the blis-

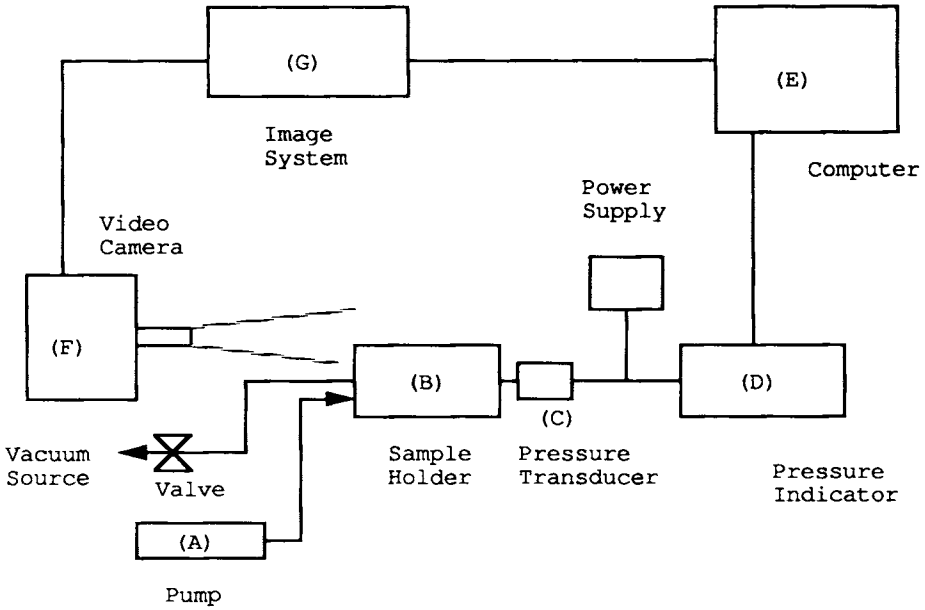

Figure 1 Schematic diagram of the experimental apparatus.

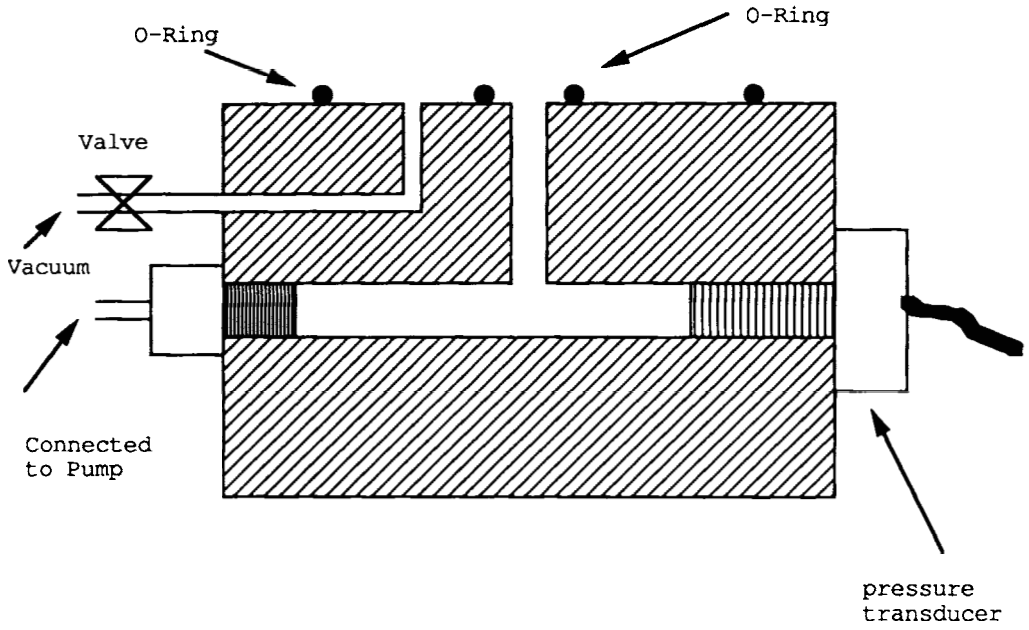

Figure 2 Schematic diagram of the sample holder.

ter is recorded by the video camera and is later measured in the image analysis system. The data from the first debonding did not show reproducibility, nor could they be modeled with the linear-elastic theory described below. On the other hand, the data from the second debonding were reproducible and closely obeyed the theoretical predictions.

THEORETICAL

The blister test was recently analyzed for a linear elastic overlayer, ignoring all dissipative effects by Gent and Lewandowski[2] based on earlier works by Hinckley,[5] Williams,[10] and Hencky.[11] Figure 3 illustrates the blister geometry. The two important

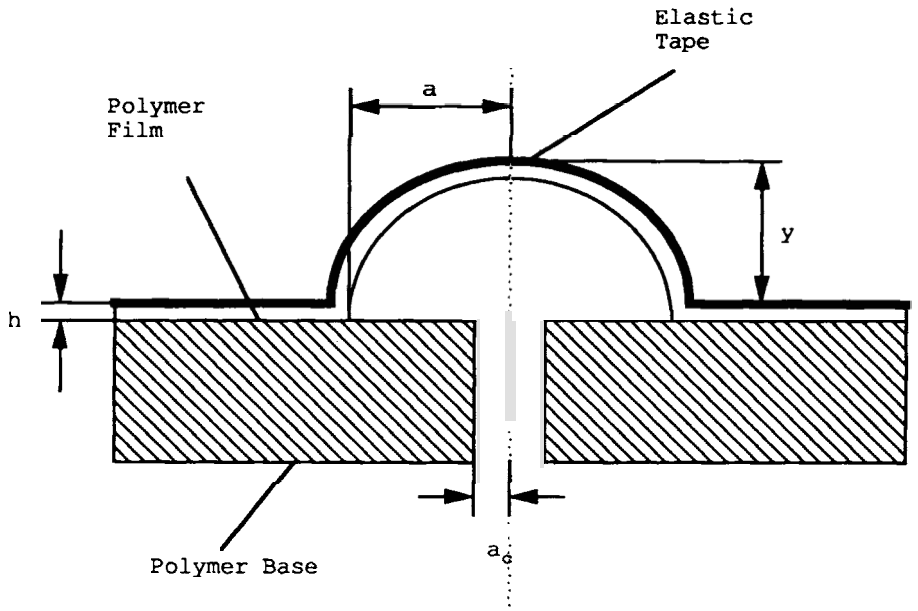

Figure 3 Schematic diagram of the blister geometry.

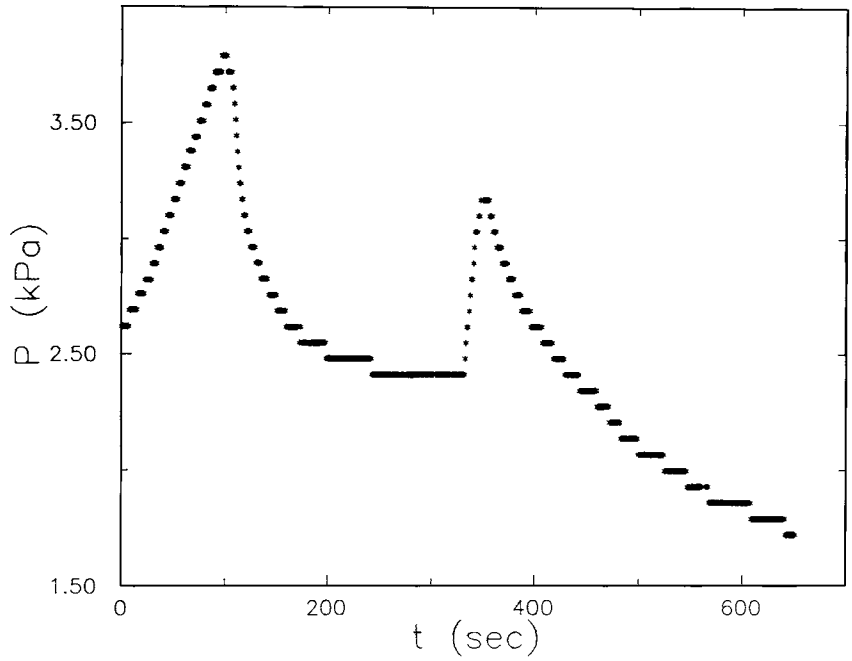

Figure 4 Representative experimental data for the debonding pressure P vs. time t.

predictions of Gent's analysis are that the product of the pressure after debonding begins, P, and the blister height, y, is proportional to the adhesion energy

$$Py = 0.649^{-1}G_a \tag{1}$$

and, at the same time, the product of the debonding pressure, P, and the blister radius, a, should be a constant involving the adhesion energy:

$$Pa = (17.4EhG_a^3)^{1/4} \tag{2}$$

Here E is Young's modulus of the overlayer and h is its thickness. Equations (1) and (2) provide a means of calculating G_a from blister test data; these have been verified experimentally by Gent and Lewandowski.[2]

The Appendix gives an analysis of a blister test carried out at a constant volumetric flow rate of the working fluid. It predicts definite relationships for the time dependence of the debonding pressure $P(t)$ [eq. (A-9)], the blister radius $a(t)$ [eq. (A-12)] and the blister height $y(t)$ [eq. (A-22)]. The key predictions are that after debonding begins, P^{-3}, a^3, and y^3 are linear in time, t. From the slopes of these linear relations, the adhesion energy can be calculated:

$$G_a = 0.39(R^2/N^2Eh)^{1/5} \tag{3}$$

$$G_a = 0.44Eh(R/M)^4 \tag{4}$$

and

$$G_a = 8.18Eh(L/R)^2 \tag{5}$$

where R is the constant volumetric rate of fluid injection, N is the slope of the P^{-3} vs. t relation, M is the slope from the a^3 vs. t relation, and L is the slope from the y^3 vs. t relation.

Since P, a, and y are measured independently, and each of the above three equations contains only

Table I Critical Pressures for First and Second Debondings

	Critical Pressure P (kPa)	
Sample	First Debonding	Second Debonding
1	3.79	3.17
2	5.03	3.10
3	4.41	3.31
4	4.89	3.24
5	5.51	3.17
Average	4.73	3.20
Standard Deviation	0.58	0.07

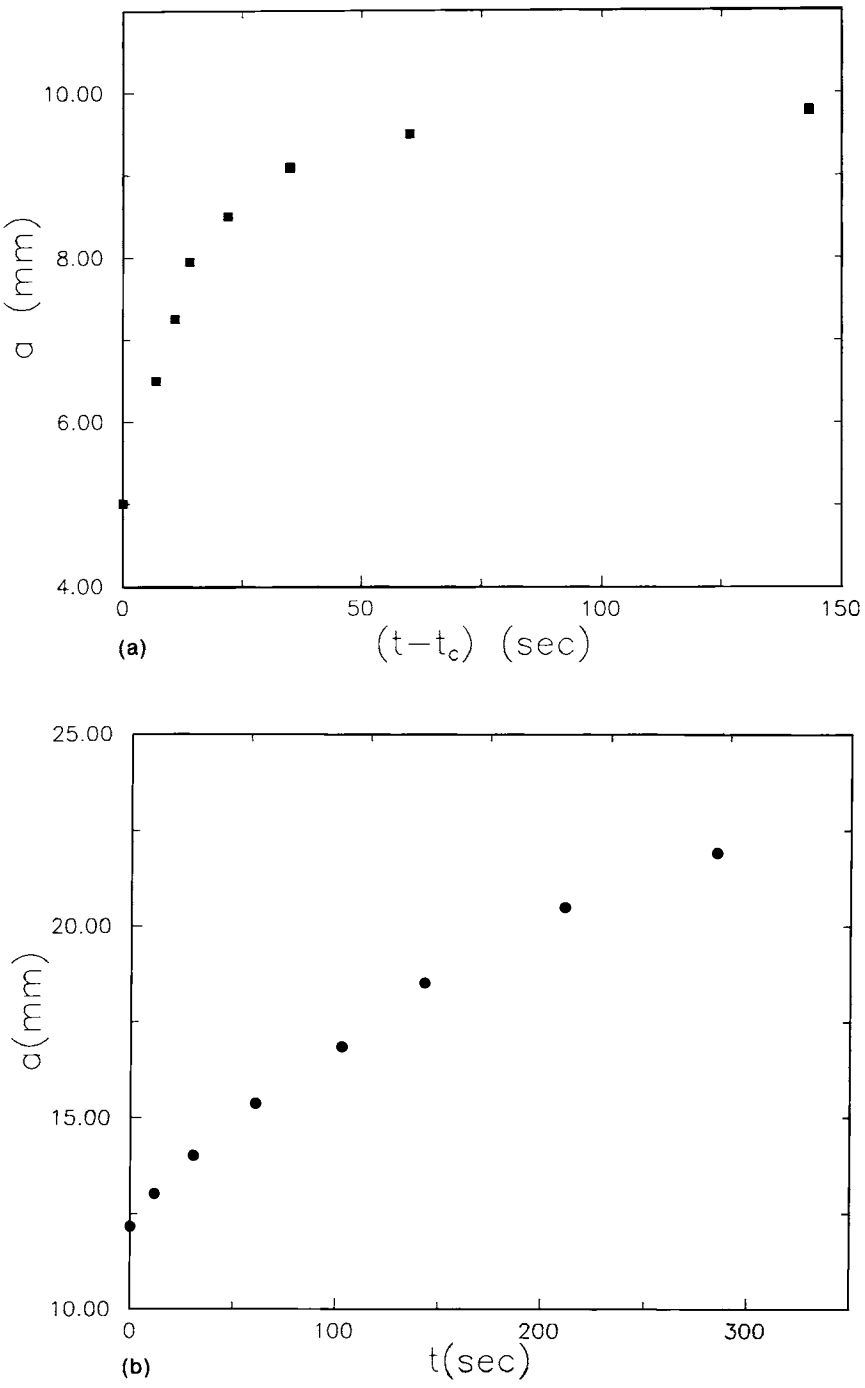

Figure 5 Representative experimental data for the blister radius a vs. time t. (a) First debonding; (b) second debonding.

one of these variables, eqs. (3)–(5) give three independent methods for calculating the adhesion energy from the time dependent debonding data. Equation (3) is especially convenient, since one does not need the geometry of the blister, which is difficult to measure.

RESULTS AND DISCUSSION

Five separate samples were prepared and tested. Figure 4 shows a typical relation for the pressure P vs. time t. The plot shows two peaks corresponding to the sequential debonding at two flow rates: 0.05

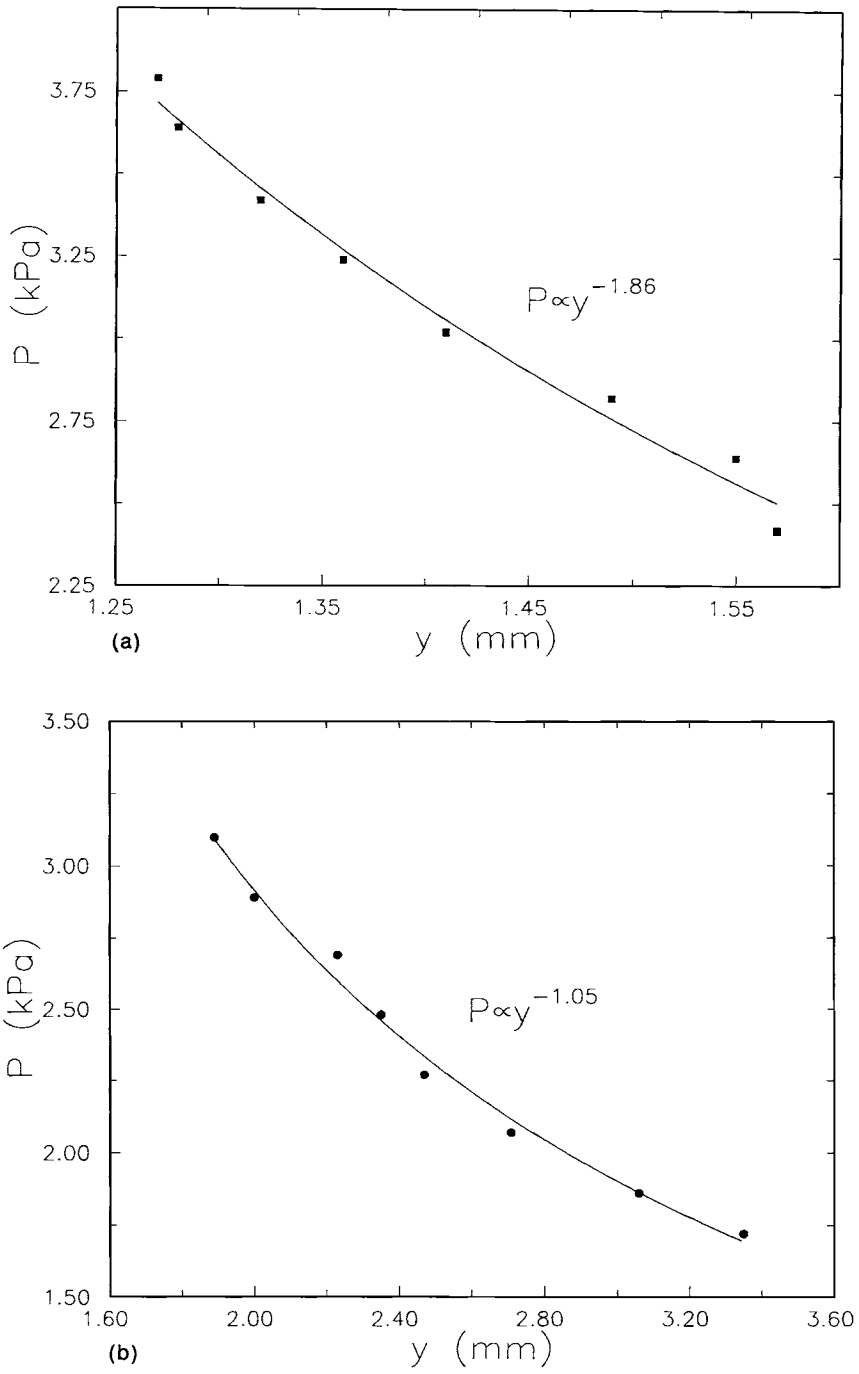

Figure 6 Representative experimental data for the debonding pressure P vs. the blister height y after debonding. (a) First debonding, (b) second debonding. The solid curves are nonlinear least squares fits.

mL/min and then 0.5 mL/min. For all the tests, the rate was changed from 0.05 mL/min to 0.5 mL/min when pressure fell to certain low value during the first debonding (P = 2.41 *kPa* was arbitrarily chosen as the low value). For the system under investigation, this corresponded to the blister being sufficiently large so that its radial growth rate would fall below about 0.1 mm/s at the larger flow rate.

The critical pressures for both debondings in each sample are given in Table I. Clearly, the reproduc-

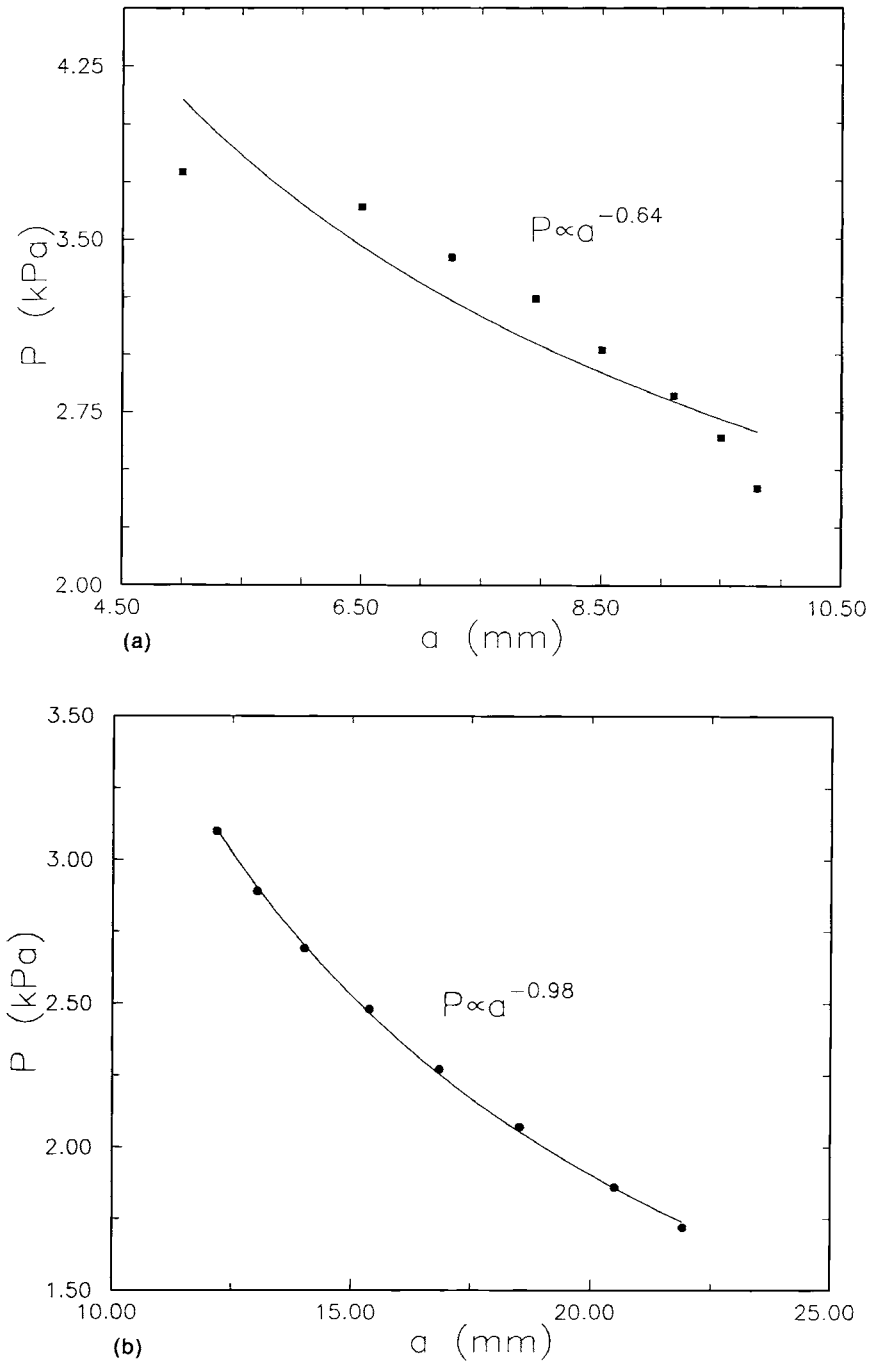

Figure 7 Representative experimental data for the debonding pressure P vs. the blister radius a after debonding. (a) First debonding, (b) second debonding. The solid curves are nonlinear least squares fits.

ibility of the critical pressure for the second debonding is excellent. On the other hand, poor reproducibility is obtained for the critical pressure in the first debonding. The reason for this is that the structure of the interface in the vicinity of the substrate perforation cannot be prepared reproducibly. However, as the debonding process proceeds, a fracture propagates along the interface, creating a fresh

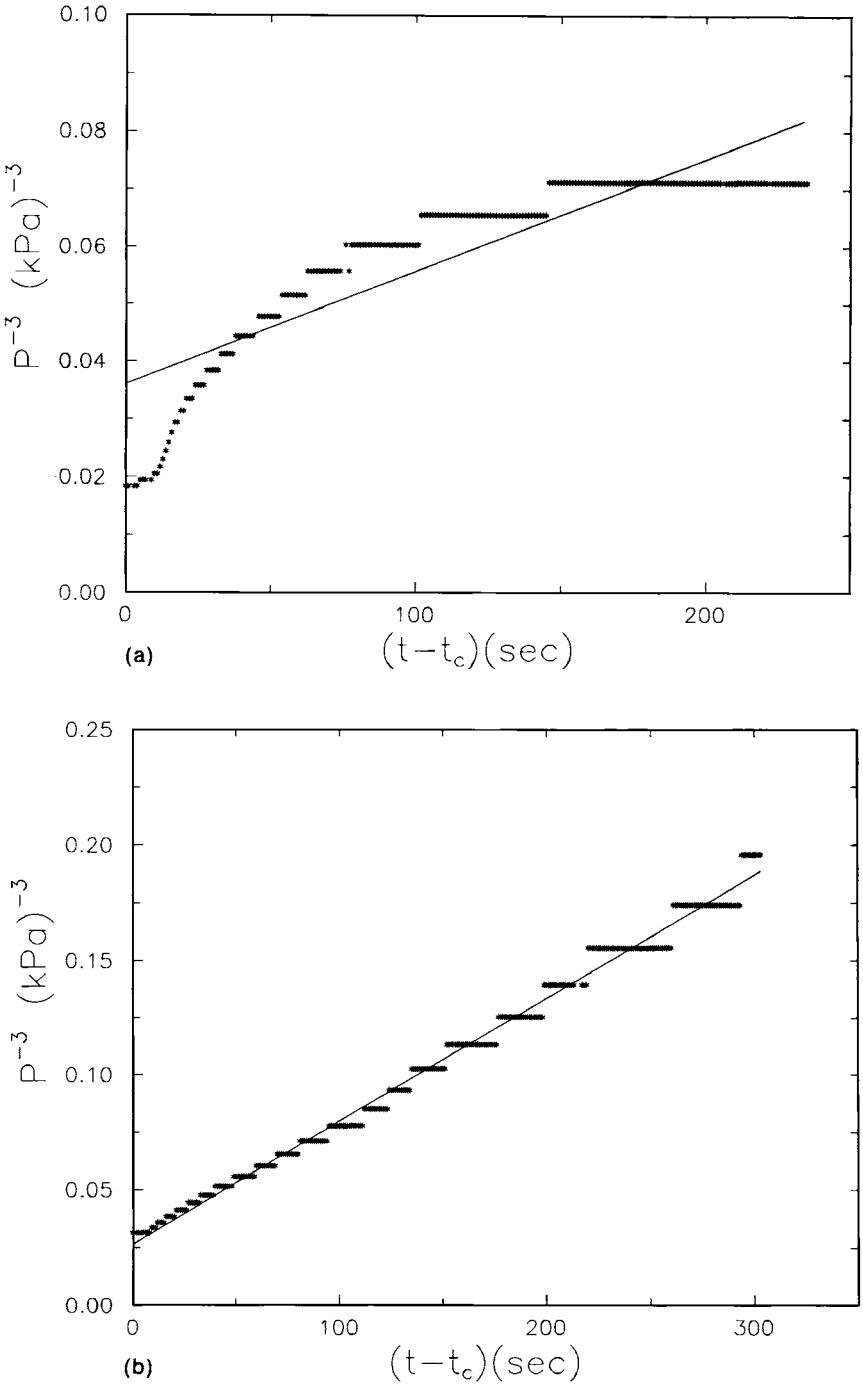

Figure 8 Representative experimental data for P^{-3} vs. time t–t_c. (a) First debonding, (b) second debonding. The straight lines are linear least squares fits.

crack tip. This structure can be reproduced reliably, and leads to consistent values of the second critical pressure.

Before proceeding, let us consider the debonding rates produced during the first and second debondings. During the first debonding, one achieves a relatively high critical pressure, after which the pressure drops very rapidly. The small initial size of the blister and, possibly, an inertial effect, causes a relatively large change of the debonding rate initially

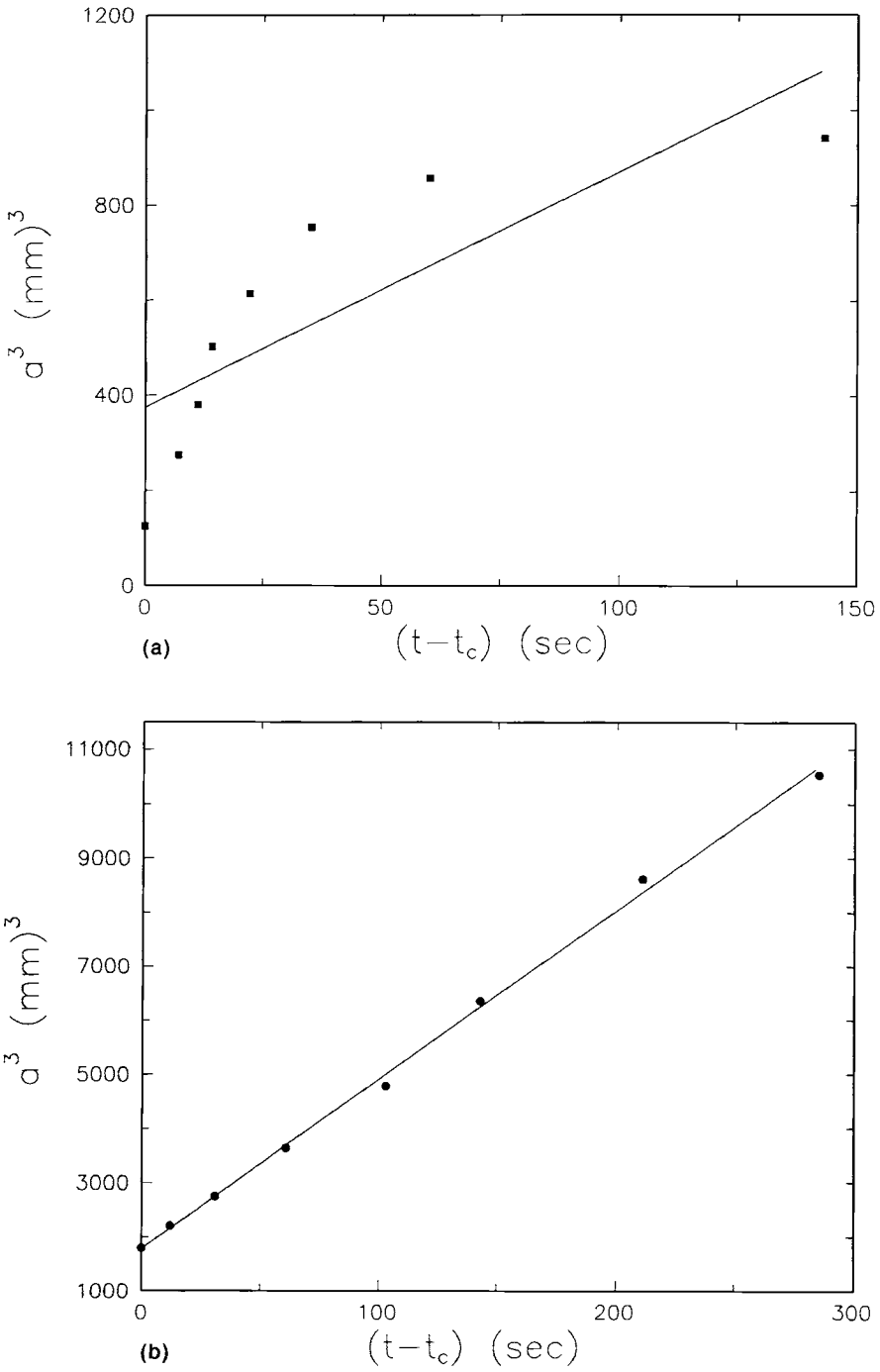

Figure 9 Representative experimental data for a^3 vs. time $t-t_c$. (a) First debonding, (b) second debonding. The straight lines are linear least squares fits.

from a large value to a much smaller value later; Figure 5(a) illustrates this with a plot of a vs. $t-t_c$, whose slope corresponds to the instantaneous debonding rate. One expects that the large rate and large variation in rate causes a large contribution in the work done by dissipative processes, which changes significantly during the experiment. This should be reflected in the data during the early stages of the process. On the other hand, during the second debonding, where the blister radius is large and the pressure falls much more slowly, the debonding rate is low and changes slowly, as shown in Figure 5(b).

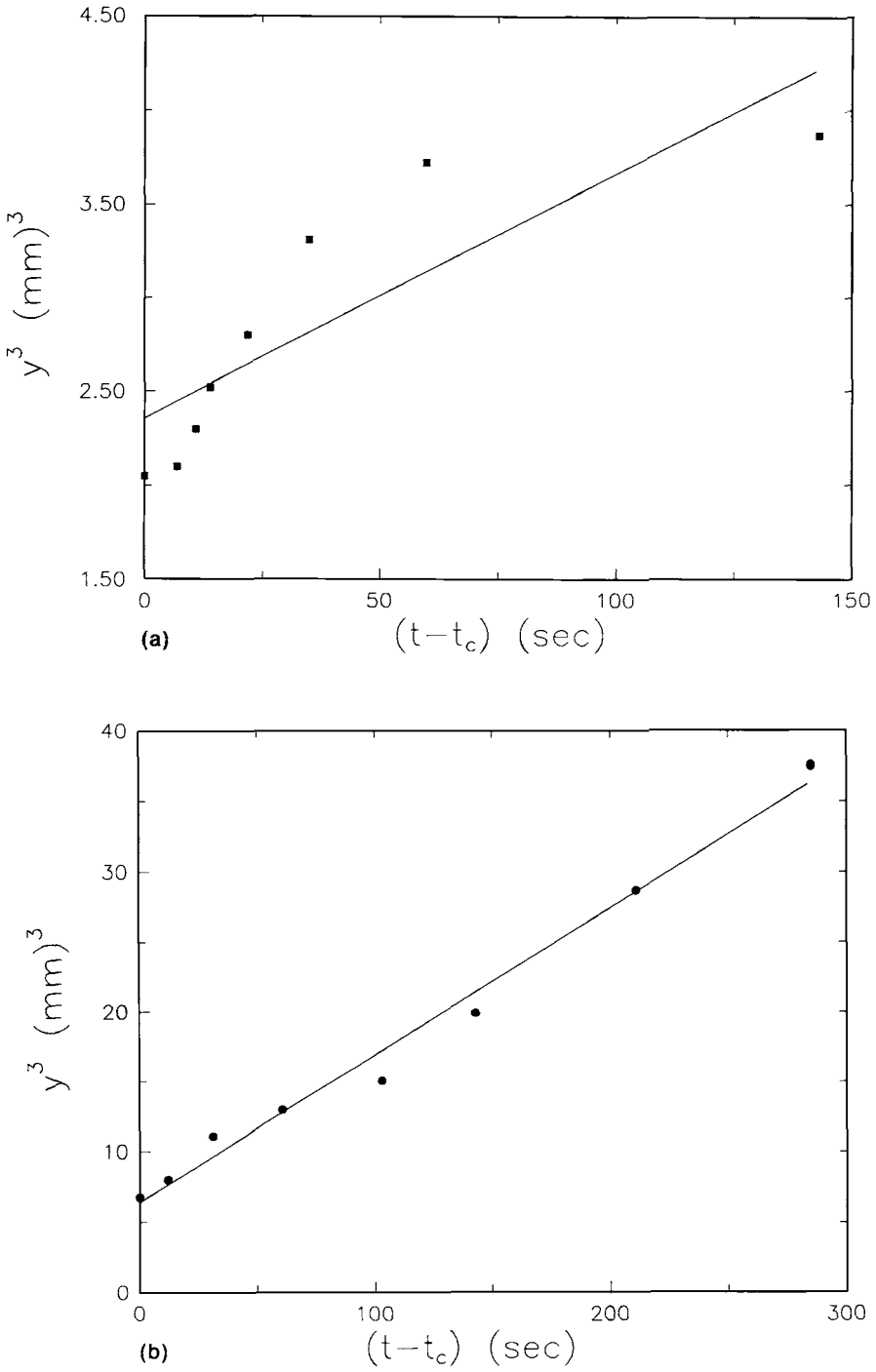

Figure 10 Representative experimental data for y^3 vs. time $t-t_c$. (a) First debonding, (b) second debonding. The straight lines are linear least squares fits.

In this case, the rate is minimal and does not vary much, so the data should follow the quasi-steady analysis more closely than data from the first debonding.

Figures 6 and 7 verify this prediction with plots of the debonding pressure P vs. blister height y and radius a, respectively, after the first and second debondings. According to eqs. (1) and (2), these plots should obey $P \alpha y^{-1}$ and $P \alpha a^{-1}$. The second debonding shows excellent agreement with the predictions, while first debonding shows poor agreement. (To illustrate this clearly, nonlinear least

squares fits of the data to power law functions are shown.) The discrepancy between the data and theory in Figures 6(a) and 7(a) is likely because of the high initial debonding rate during the first debonding. As a result, the products Py and Pa have larger values than expected initially and smaller values later. This effect was also encountered by Gent and Lewandowski[2] in experiments with elastic tapes as an overlayer.

Figures 8, 9, and 10 show representative plots of P^{-3}, a^3, and y^3 vs. debonding time $t-t_c$, respectively, for both first and second debondings. According to eqs. (A-9), (A-12), and (A-22), linear relations should be found. Again, data from the second debonding show excellent agreement with the predictions, while poor agreement is obtained from data in the first debonding. Clearly, during the first debonding, the quasi-steady linear–elastic theory is not obeyed. Figures 8, 9, and 10 also include linear least squares fits, which underscore the qualitative differences between data during the first and second debondings.

The adhesion energy calculated from eqs. (1)–(5) for second debondings are listed in Table II. Equations (3)–(5) give self-consistent values for G_a, strongly supporting the theory and the experimental approach. Ahagon and Gent[7] carried out peel tests on a similar system (polybutadiene/Pyrex glass) using different peel rates. They calculated fracture energies at zero peel rate by extrapolation. Values in the range 1.5–2.0 N/m were found, which are of the same order of magnitude as in our experiments. Helfand and coworkers[12,13] developed the mean-field theory of polymer–polymer interfaces. They found a relation between the interfacial tension and the interfacial thickness, which allows estimation of the true, thermodynamic adhesion energy for the interface. Their relation can be expressed approximately as follows:

$$r = Bm^n \tag{6}$$

where the interfacial tension, r, is expressed in N/m, and the interfacial thickness m is expressed in Å. B and n have values on the order of 0.1 and -1, respectively. For NR/PMMA, m is on the order of 10 Å. Thus, from eq. (6), one finds an adhesion energy for NR/PMMA on the order of 0.1 N/m. Clearly, the adhesion energies listed in Table II include dissipative contributions, although these are relatively minor when compared with those found in conventional peel tests.

Table II Adhesion Energies Calculated from Eqs. (1) to (5) for Second Debonding

	G_a (N/m)				
Sample	Eq. (1)	Eq. (2)	Eq. (3)	Eq. (4)	Eq. (5)
1	3.71	3.60	3.93	4.02	3.63
2	3.67	3.51	3.97	3.99	3.87
3	3.53	3.69	4.03	3.92	3.75
4	3.77	3.70	3.99	4.00	3.96
5	3.69	3.66	3.91	3.94	3.83
Average	3.67	3.63	3.97	3.97	3.81
Standard Deviation	0.08	0.07	0.04	0.04	0.11

Debonding rate is about 0.07 mm/sec.

CONCLUSIONS

A blister test experiment was designed and applied to the study of NR/PMMA interfacial adhesion. The initial study leads to the following conclusions:

1. In order to minimize the dissipative effects caused by relatively large initial debonding rates, a sequential debonding procedure can be used. Here, a blister is grown to a large radius at a low flow rate; debonding is then reinitiated. This gives a reproducible crack tip, leading to reproducible critical pressures, and yields low, slowly varying, radial growth rates, which evidently minimize the influence of dissipation on the quasi-steady data, allowing a quasi-steady analysis by linear–elastic theory. One should keep in mind that dissipation is always present in the blister test; its effect is only to alter the value of the adhesion energy, G_a, when one employs the sequential debonding process.
2. An energy balance analysis reveals the relationships for the time dependence of the debonding pressure, P, the blister radius, a, and the blister height, y, during a test carried out at a constant fluid injection rate. The predictions are that after debonding begins, P^{-3}, a^3, and y^3 are linear in time t. The slopes of these linear relations are directly related to the adhesion energy.
3. From this analysis and the analysis of Gent and Lewandowski,[2] five different methods can be applied to calculate the adhesion energy G_a.

4. The self-consistency of fracture energies calculated in this study suggests that G_a can be calculated reliably from the pressure data alone without using the blister geometry, which is difficult to measure.

The authors thank Professors E. F. Leonard and C. C. Gryte at Columbia University for providing access to their laboratory facilities. The authors also thank Mr. R. Heffner at Columbia Chemical Engineering Shop, and Mr. T. Y. Zhang at Lawrence Berkeley Laboratories, for helping with the experimental set up. Finally, the authors thank Mr. S. Dalpe at Exxon Chemical Company for measuring the Young's modulus of the NR overlayer.

APPENDIX

For a linear elastic overlayer fixed to the substrate along a circular periphery, previous works[2] show that the blister inflation obeys the following equations:

$$V = C_1\pi a^2 y \tag{A-1}$$

and

$$y = C_2(Pa^4/Eh)^{1/3} \tag{A-2}$$

where V is the volume of the blister, y is its height, and a is its radius. Also, h is the thickness of the overlayer, P is the inflation pressure, and E is Young's modulus of the overlayer. C_1 and C_2 are material constants; for incompressible overlayers, $C_1 = 0.519$ and $C_2 = 0.595$.

Differentiating eq. (A-1) with respect to time yields

$$dV/dt = C_1\pi a^2 dy/dt + 2C_1\pi a y\, da/dt$$

If the volume increases at a constant rate R, the above equation can be written as

$$dy/dt = R'/a^2 - (2y/a)da/dt \tag{A-3}$$

where $R' = R/C_1\pi$.

Similarly, a time derivative of eq. (A-2) gives

$$3dy/dt = C_2(Eh)^{-1/3}a^{4/3}P^{-2/3}dP/dt + 4C_2(Eh)^{-1/3}(Pa)^{1/3}da/dt \tag{A-4}$$

Substituting (A-3) into (A-4), and using (A-2), we get

$$3R'/a^2 - 10C_2(Pa/Eh)^{1/3}da/dt = C_2(Eh)^{-1/3}(Pa)^{-2/3}a^2 dP/dt \tag{A-5}$$

From Gent and Lewandowski's[2] analysis, one has

$$Pa = (17.4EhG_a^3)^{1/4} = K = \text{constant} \tag{A-6}$$

Therefore

$$da = (-K/P^2)dP \tag{A-7}$$

Substituting (A-7) into (A-5), and simplifying, yields

$$-(3A/P^4)dP = (R'/K^3)dt \tag{A-8}$$

where $A = C_2(K/Eh)^{1/3}$. Equation (A-8) can be integrated to give

$$P^{-3} = (R'/AK^3)(t-t_c) + P_c^{-3} \tag{A-9}$$

where t_c is the time when debonding begins and P_c is the critical pressure. From eq. (A-9), a plot of P^{-3} vs. $t-t_c$ should be a straight line with slope

$$N = R'/AK^3 \tag{A-10}$$

From eqs. (A-10) and (A-6), we get

$$G_a = 0.39(R^2/N^2Eh)^{1/5} \tag{A-11}$$

Similarly, we can also get

$$a^3 = (R'/A)(t-t_c) + a_c^3 \tag{A-12}$$

where a_c is the radius of the blister when debonding first begins. If we plot a^3 vs. $t-t_c$, one expects a linear relation with slope

$$M = R'/A \tag{A-13}$$

Equations (A-13) and (A-6) yield

$$G_a = 0.44Eh(R/M)^4 \tag{A-14}$$

Now, let us rewrite eqs. (A-2) and (A-3); we get

$$a = (y^{3/4}(Eh)^{1/4})/(C_2^{3/4}P^{1/4}) \tag{A-15}$$

$$da/dt = R'/2ay - (a/2y)dy/dt \tag{A-16}$$

Substituting (A-16), then (A-15), into (A-4) and simplifying, yields

$$5dy/dt = yP^{-1}dP/dt + 2C_2^{3/2}R'(Eh)^{-1/2}P^{1/2}y^{-3/2} \quad \text{(A-17)}$$

From Gent and Lewandowski's[2] analysis, one has

$$Py = (4/5C_1)G_a = J = \text{constant} \quad \text{(A-18)}$$

Therefore,

$$P = J/y \quad \text{(A-19)}$$

and

$$dP = -Jy^{-2}dy \quad \text{(A-20)}$$

Substituting (A-19) and (A-20) into (A-17), and simplifying, yields

$$3y^2dy = C_2^{3/2}R'(Eh)^{-1/2}J^{1/2}dt \quad \text{(A-21)}$$

The above equation can be integrated to yield

$$y^3 = C_2^{3/2}R'(Eh)^{-1/2}J^{1/2}(t-t_c) + y_c^3 \quad \text{(A-22)}$$

where y_c is the blister height when debonding begins. So, a plot of y^3 vs. $t-t_c$ should be a straight line with slope

$$L = C_2^{3/2}R'(Eh)^{-1/2}J^{1/2} \quad \text{(A-23)}$$

From eqs. (A-18) and (A-23), we get

$$G_a = 8.18Eh(L/R)^2 \quad \text{(A-24)}$$

Eqs. (A-11), (A-14), and (A-24) give three alternative independent methods for calculating the adhesion energy.

REFERENCES

1. K. S. Kim and J. Kim, *Trans ASME J. Eng. Mater. Tech.*, **110,** 266 (1988).
2. A. Gent and L. Lewandowski, *J. Appl. Polym. Sci.*, **33,** 1567 (1987).
3. H. Dannenberg, *J. Appl. Polym. Sci.*, **5,** 125 (1961).
4. M. Napolitano, A. Chudnovsky, and A. Moet, *J. Adhesion Sci. Technol.*, **2,** 311 (1988).
5. J. Hinckley, *J. Adhesion,* **16,** 115 (1983).
6. M. Allen and S. Senturia, *ANTEC '88,* 997 (1988).
7. A. Ahagon and A. Gent, *J. Polym. Sci. Polym. Phys. Ed.*, **13,** 1285 (1975).
8. A. Gent and R. Petrich, *Proc. Roy. Soc.*, **A310,** 433 (1969).
9. T. Igarashi, *J. Polym. Sci. Phys. Ed.*, **13,** 2129 (1975).
10. M. Williams, *J. Appl. Polym. Sci.*, **13,** 29 (1969).
11. H. Hencky, *Zr. Math. Phys.*, **63,** 311 (1915).
12. E. Helfand and Y. Tagami, *J. Chem. Phys.*, **56,** 3592 (1971).
13. E. Helfand and A. Sapse, *J. Chem. Phys.*, **62,** 1327 (1975).

Received July 31, 1991
Accepted September 4, 1991